Dynamic monitoring of civil infrastructures with geodetic sensors

Caroline Schönberger, Werner Lienhart, Thomas Moser

Institute of Engineering Geodesy and Measurement Systems, Graz University of Technology, Steyrergasse 30, 8010 Graz, Austria, (c.schoenberger@tugraz.at; werner.lienhart@tugraz.at; thomas.moser@tugraz.at)

Key words: *dynamic monitoring*; *global navigation satellite system*; *robotic total stations, structural health monitoring*

ABSTRACT

Geodetic sensors are conventionally used for the long-term monitoring of civil structures like bridges, buildings or water dams. With the recorded data the reaction of the structure to slow changing impacts like temperature changes can be observed. However, the reaction due to dynamic impacts like wind loads, traffic loads or earthquakes are usually assessed using non-geodetic sensors like accelerometers. This article discusses how advances in geodetic sensing technology opens up new possibilities. In laboratory tests and on a real footbridge, it is demonstrated that modern total stations and GNSS receivers are well suited for the dynamic monitoring of bridges. It is shown that even small amplitudes in the range of about 1 mm for GNSS and of about 0.2 mm for total stations depending on the distance to the object can be detected.

I. Introduction

Monitoring of civil structures can be carried out as static and quasi-static displacement monitoring or by monitoring the dynamic characteristics. For the latter, usually accelerometers are applied on structures to derive its dynamic characteristics induced by wind loads, traffic loads or earthquakes. With advances in geodetic sensing, dynamic responses could also be observed with those sensors (Im *et al.*, 2013).

Global Navigation Satellite Systems (GNSS) are around for more than three decades, and in the recent years dynamic GNSS monitoring for bridges (Moschas and Stiros, 2011), towers (Górski, 2017) and buildings (Yi *et al.*, 2013) where carried out. They show eigenfrequencies below 5 Hz with displacements of 10 – 20 mm.

Advantages of GNSS in structural health monitoring (SHM) are continuous, weather-independent 3D measurements, in real time. Furthermore, no line of sight needs to be established. On the other hand, limitations of accuracy for GNSS measurements are multipath errors, satellite geometry, and a low sampling rate (Shen *et al.*, 2019).

A modern Robotic Total Station (RTS) is able to lock onto a reflector target and follow it automatically (Lienhart *et al.*, 2017). Therefore, a line of sight, as well as a stable total station position are necessary. The inbuilt tilt sensor as well as standard total station features like free stationing allows to monitor the total station position itself.

For deriving the dynamic characteristics, a transformation of the data time series into the frequency domain is needed. Potential approaches are Wavelet Analysis, Fast Fourier Transformation (FFT) or Short Time Fourier Transformation (STFT).

Depending on the data rate, frequencies up to the half of this rate can be derived from this data (Shannon, 1949). Frequencies above this value will be seen as aliasing effect, if they are not filtered out.

This paper will focus on the applicability of GNSS and RTS for dynamic monitoring, its accuracy and limitation, with experiments under controlled laboratory conditions and at a footbridge.

II. Experiments in Laboratory Setup

A. *GNSS Experiment at rooftop laboratory*

The experiment took place at the rooftop laboratory, with very few obstacles to the sky, at TU Graz. A Leica GS18 receiver was setup as a reference on a stable pillar. A Leica GR30 receiver with an AS10 antenna was used as rover. The rover antenna was placed on an APS 400 shaker (Figure 1), which is able to generate controlled oscillations. This experiment covers the vertical acceleration of a frequency range of 1-10 Hz with accelerations from 0.3 to 16 m/s². Both receivers recorded GPS (G), GLONASS (R) and GALILEO (E) signals with a data rate of 20 Hz.

Figure 1. Experiment setup at the rooftop laboratory. Monitoring site with shaker (left), reference site (right).

Additionally, observation data from the Austrian reference network, Austrian Positioning Service (APOS), station GRAZ was used in the analysis. This station is located in around 3 km distance to the laboratory and provides GPS and GLONASS data with 1 Hz.

To compare the results of the GNSS data, the shaker movement was additionally measured very precisely with a laser triangulation sensor (LTS). Its data rate is 312.5 Hz and the data is used as true values.

First, 7.5 minutes of (1) no motion were recorded. Then (2) the shaker was operated in certain frequencies with various amplitude steps, where every frequency-amplitude combination was hold for 50 seconds before starting the next combination. Lastly, (3) a linear sweep from 10 Hz to 0.8 Hz in 2 minutes was carried out.

The data processing chain is shown in Figure 2. The RINEX data of the reference and the rover were processed in postprocessing mode with RTKLIB 2.4.2 (Takasu, 2011) and Leica Infinity 2.4.1 using broadcast ephemeris. On those results an outlier detection using a moving median method (Le Thi, 2021) and a high-pass Chebyshev filter with an edge frequency of 0.05 Hz, to exclude the impact of long-term effects, was applied (Moschas and Stiros, 2011). To transfer the data into the frequency domain an FFT and STFT were carried out.

Figure 2. GNSS data processing chain.

The results in this paper focus on the height component of the data as this is often the most relevant in bridge monitoring.

1) No Motion: This data is used to compare combinations of data rate at the reference, used satellite signal, postprocessing program and the use of data from a reference network by comparing its standard deviation.

The data rate of the local reference station was down sampled with GFZRNX (Nischan, 2016) to 1Hz, 5 s and 30 s, which are common intervals for reference network stations and hence possible real time intervals.

A data rate – reference combination was processed with both programs, with only-GPS (G) or GPS and GLONASS (GR) for the APOS reference or GPS, GLONASS and GAL (GRE) for the local reference station.

The standard deviation (STD) of those time series was calculated to quantify the background noise and it is shown in Figure 3.

The best result could be achieved for the local reference with a data rate of 20 Hz and the satellite systems GRE (GRE20Hz). An increased STD could be observed with a reduced reference data rate, especially for multi-GNSS for RTKLIB. For all combinations with a STD of less than 5 mm, RTKLIB results are better.

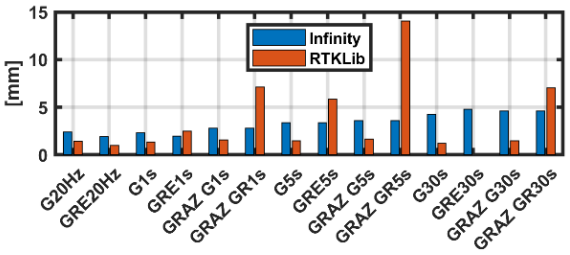

Figure 3. Standard deviation in vertical direction for the time series of no motion.

Calculating an FFT over the GRE20Hz data set, Figure 4, shows noise with a good distribution over the whole frequency domain, and the cut off the low frequencies with the high-pass filter. There is no significant noise on the data recorded by the LTS. Less noise in the RTKLIB results compared to the results from Infinity is clearly visible.

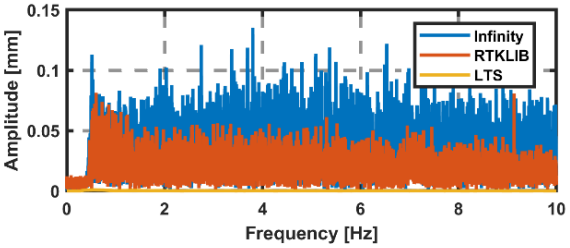

Figure 4. FFT over the no motion part (GRE20Hz) shows noise with a good distribution over the whole frequency domain.

The FFT over the same time period for only GPS and a local reference with a data rate of 5 s (G5s) shows artefacts in the frequency domain, Figure 5. A closer look at a small selection of the time series, Figure 6, show abrupt changes introduced by the reference data rate. The impact of those changes is seen in the frequency domain.

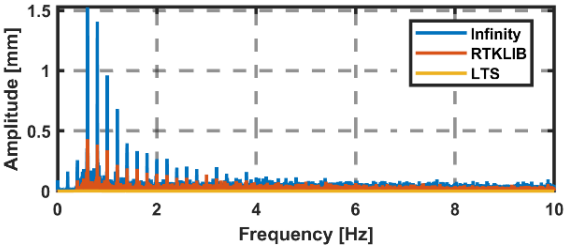

Figure 5. FFT over the no motion part (G5s) shows artefacts in the frequency domain introduced by the reference data rate.

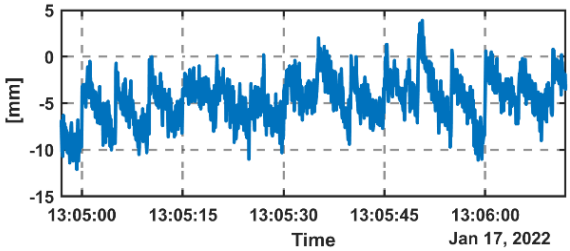

Figure 6. Section of the original time series with a reference data rate of 5 s. Abrupt changes in the data can be seen, which conclude to artefacts in the frequency domain.

Due to the lowest standard deviation in the no motion part and no appearance of unwanted pattern in the frequency domain, the GRE20Hz data set is used for the following research.

2) Amplitude - frequency steps: For every frequency-amplitude combination an FFT was calculated. The results of the frequencies: 2 Hz, 5 Hz and 9 Hz are shown in Figure 7, due to a good distribution over the frequency domain.

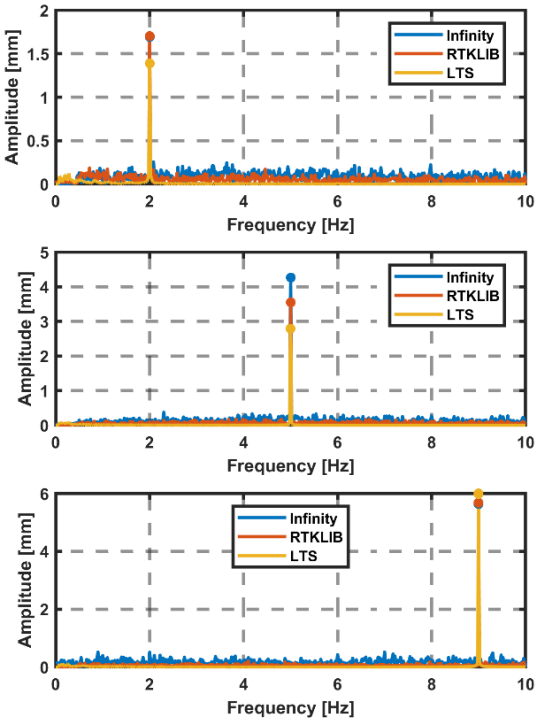

Figure 7. FFTs of GNSS and LTS data over a 50 s period with the frequencies 2 Hz, 5 Hz and 9 Hz.

Calculating the main frequency of the time series works very well for GNSS and LTS measurements. There is a slight difference in the amplitude, especially at 5 Hz. But even amplitudes with less than 2 mm could be calculated well.

3) Sweep: Figure 8 shows an FFT over the whole sweep, with the LTS as a reference. All frequencies between 10 Hz and 0.8 Hz could be recorded by the sensors.

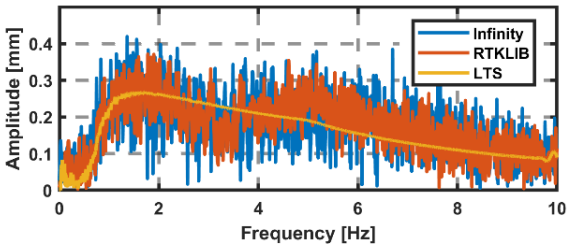

Figure 8. FFT over the whole sweep.

Due to the rapid changes of frequency and amplitude an additional STFT calculated. The block size influences the time and frequency resolution. A long block, low time resolution, results in a good frequency resolution. For this sweep a block size of 5 s was chosen.

Figure 9 shows a very good frequency calculation for GNSS data for frequencies less than 10 Hz. The amplitude fits the real values well at all frequencies below 2 Hz and over 8 Hz. Between 2 and 8 Hz the amplitude can be too low or too high.

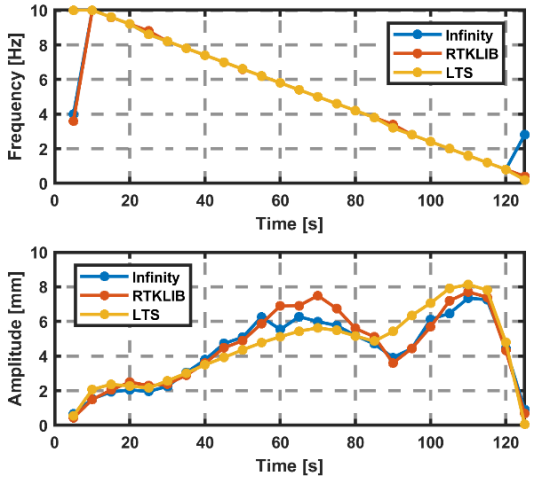

Figure 9. Amplitude and frequency of the sweep over time, calculated with a STFT with block size of 5 s.

B. *Total station experiment at rooftop laboratory*

For this study a Leica MS60 was used which is able to carry out dynamic angle measurements with up to 20 Hz and a geometric precision of 3 cc (Leica, 2020).

It is positioned around 25 m from the shaker, on a pillar with a nearly horizontal sighting to the prism, and controlled by a serial GeoCom Interface with Python surrounding. One full static measurement was carried out to receive a reliable slope distance. For the dynamic data gathering only angle measurements are used for more stable time resolution results. The data is processed with MatLab R2018a. For all FFTs the data is filtered through a high - pass filter with a cut-off frequency of 0.5 Hz.

Again, the LTS measurements, but also the data from the acceleration sensors are used as reference data.

1) No Motion: Figure 10 shows the time series of a period of time while no active movement occurs. This helps to get an idea of the atmospheric influences on the measurement path.

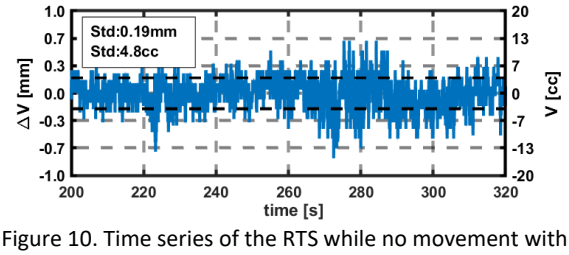

Figure 10. Time series of the RTS while no movement with its standard deviation.

The standard deviation of about 4.8 cc in angle deviation results in an observable movement of about 0.2 mm for the given slope distance of 25.265 m. Smaller movements will be covered by atmospheric noise and therefore are not possible to detect.

2) Amplitude - frequency steps: Figure 11 shows FFTs over the same amplitude – frequency combinations as shown in Figure 7.

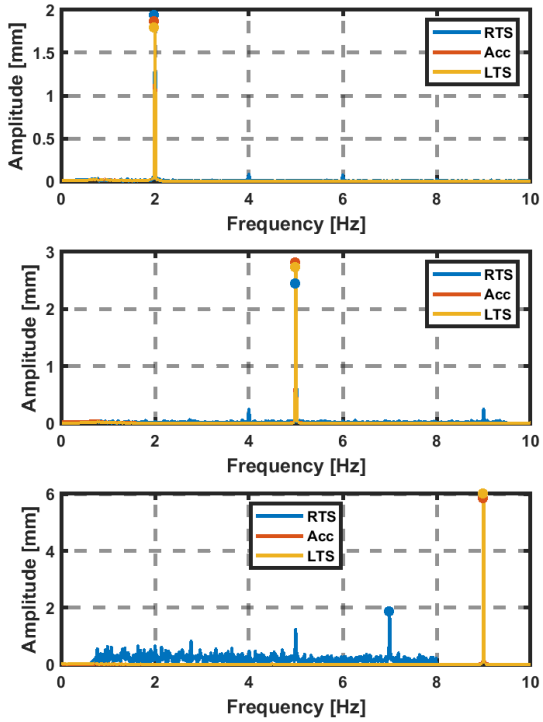

Figure 11. FFTs of RTS, LTS and Acceleration Data over a 50 s period with frequencies 2 Hz, 5 Hz, 9 Hz.

It can be seen, that a frequency of 9 Hz cannot be detected by the RTS. This is due to the fact, that the measurement rate went down to 16 Hz in this time period. Therefore, only frequencies up to 8 Hz can be detected. The drop of the measurement rate seems to be dependent to the ratio of amplitude and frequency of the target. Especially when there are fast direction changes, the RTS has its problems to follow the target. Still, there is a peak at 7 Hz, which is due to the aliasing effect.

Anyways, lower frequencies can be detected flawlessly, as well as the measurement rate goes back up as the movement slows down.

3) Sweep: Figure 12 shows an FFT over the whole sweep.

The noise of the RTS is much higher than the noise of other sensors. Still the amplitude and frequency can be detected. Also, the measurement rate stays up to 20 Hz in this experiment, therefore the frequency can be detected up to 10 Hz.

In Figure 13 the time series of the sweep is analysed using a SFTF with a block size of 5 s, equivalent to Figure 9.

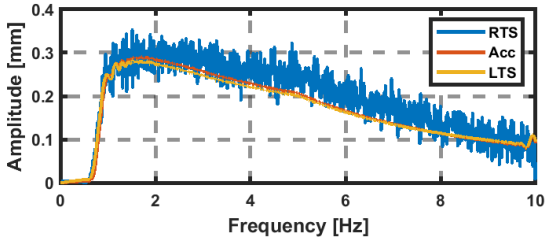

Figure 12. FFT of RTS, LTS and Acceleration Data over the whole sweep.

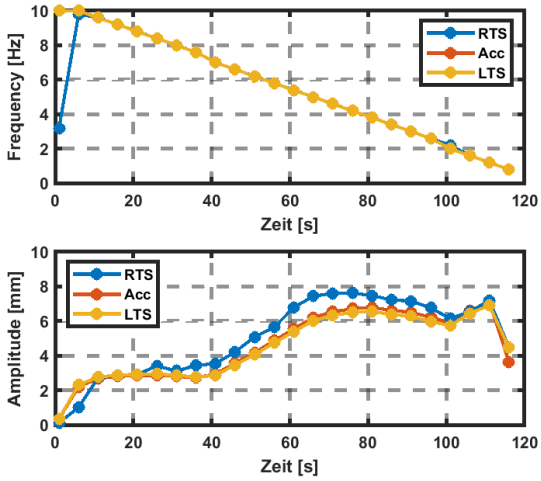

Figure 13. Amplitude and Frequency of the Sweep over time for RTS, LTS and Acceleration sensor, block size 5 s.

The RTS has some problems with following the frequency of 10 Hz, but manages to trace all following frequencies. The amplitude is mostly overshot by the RTS. This phenomenon increases with increased amplitude, except for very low and very high frequencies. It can be said, that some critical combination of amplitude and frequency can lead to troubles with following the target exactly. This and the drop of the measurement rate at some situations are the main issues of this test.

III. Dynamic Monitoring on a Footbridge

For a real-world test scenario, a nearby public footbridge with a length of around 70 meters was chosen. Different sensorics: GNSS, IMU, accelerometers, prism and image targets were placed on the bridge. The prism was traced by an RTS from a closed by bank and the image target was filmed by a camera from the river bank. Figure 14 shows a schematic representation of the measuring setup and Figure 15 shows a photo taken from the bank.

Around 2 hours of data were recorded including the excitement of the bridge by 15 students jumping over the bridge, 2 people jumping and 1 minutes of no human excitation. The rest was randomly walking people passing by.

A. *GNSS + IMU*

After the very promising results in Section II A, useful results were expected on the footbridge. The Leica

GNSS receiver GR30 with an AS10 Antenna and an IMU (Epson G370N), were mounted in the middle of the bridge, where the highest amplitudes were expected. As a reference a Leica GS18 was located on solid ground. Both receivers recorded GPS, GLONASS and GALILEO signals with a data rate of 20 Hz and the data rate of the IMU was 200 Hz.

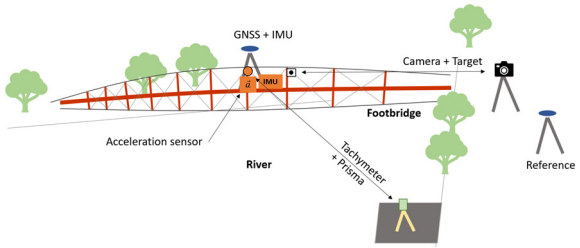

Figure 14. Schematic representation of the measurement setup at a public footbridge in Graz, including GNSS, IMU, RTS, acceleration and camera measurements.

Figure 15. Photo of the measurement setup from the closed by bank, where the RTS was located.

The data processing passed trough the same data processing algorithm, as the laboratory experiment.

Figure 16 shows a waterfall plot over the experiment time, were 15 students excited the bridge, with a block size of 5 s, where the frequencies can be found on the ordinate and the amplitudes are color coded. The jumps can be seen clearly with amplitudes of up to 11 mm (bright dots).

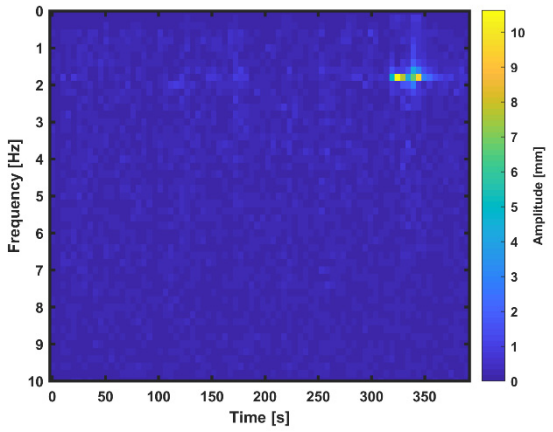

Figure 16. A waterfall diagram over the experiment time of 15 students jumping. The highest amplitudes can be seen around 1.7 Hz, during the time of jumping (320 s - 360 s).

To calculate displacements from the IMU (Z-axis) data, the data was integrated twice. The eigenfrequency of the bridge could be derived via GNSS data to 1.74 Hz, which is confirmed by the IMU data, with the same result, see Figure 17.

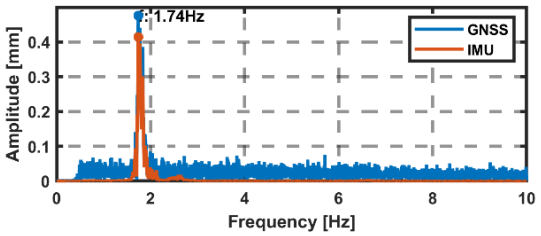

Figure 17. FFT of GNSS and IMU while 15 students jumping on the bridge. For the IMU data a zoom from 1-10 Hz was applied for a better comparison.

Figure 18 shows the amplitudes of the displacement for GNSS and IMU data at the frequency of 1.74 Hz in vertical direction. The jumps can be seen clearly with an amplitude of up to 11 mm.

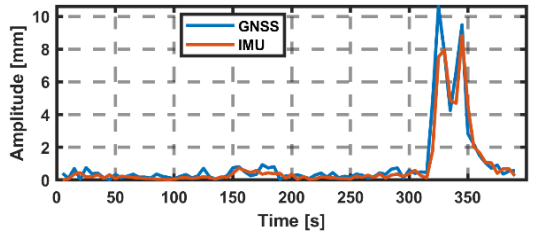

Figure 18. GNSS and IMU Time Series of the amplitude at the derived eigenfrequency of 1.74 Hz.

Both the GNSS and IMU (Z-axis) displacements are very similar and therefore reliable.

Figure 19 shows a waterfall diagram over a 5 minute period where 2 people jumped to excite the bridge. Lower amplitudes compared to the 15 students jumping are expected and it can be seen, that even with amplitudes of around 1 mm the frequencies around 1.7 Hz are dominant. Due to the smaller amplitudes, noise has a bigger impact on the data.

An FFT over this time period still show a main frequency of 1.74 Hz, Figure 20, but the difference between noise and the peak is smaller.

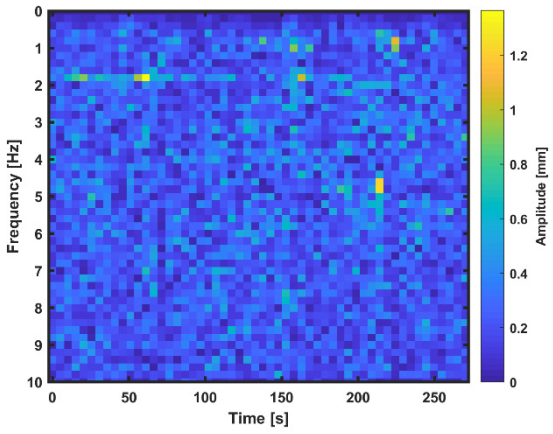

Figure 19. A waterfall diagram over the experiment time of 2 people jumping. Although the amplitudes are below 2 mm, the frequencies around 1.7 Hz are dominant.

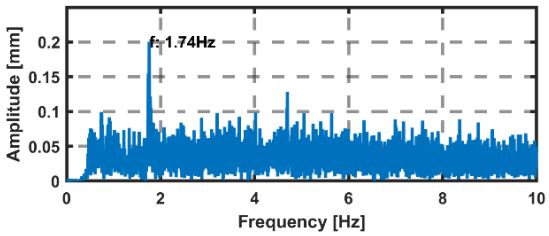

Figure 20. FFT of GNSS while 2 people jumping on the bridge.

Therefore, it can be concluded that even a small excitation, small amplitudes, can be recorded with GNSS and it is a useful technology for dynamic monitoring.

B. *Total Station and acceleration Sensor*

In this experiment the RTS is positioned 49.58m from the target which is mounted in the middle of the bridge. In Figure 21 a time series of 90 seconds is shown, where no movement at all occurs on the bridge. The RTS data is compared to the accelerometer data.

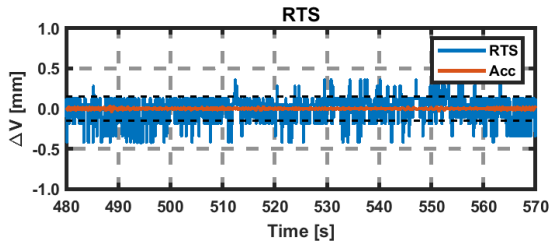

Figure 21. Time series of RTS and acceleration sensor while no movement of the bridge. STD_{RTS}: 0.15 mm, STD_{ACC}: 0.01 mm.

The acceleration sensor detects almost no movement at all, while the RTS senses random movement over the same period of time. This can be tied to the resolution of the RTS measurements but also to atmospheric disturbances. Due to the fact of very mild measurement weather, the disturbances are quite low. The standard deviation of 0.15 mm gives an idea of the smallest detectable amplitude.

In Figure 22 the time series of RTS and acceleration data is shown. Again, the event of the students jumping is clearly seen in the figure.

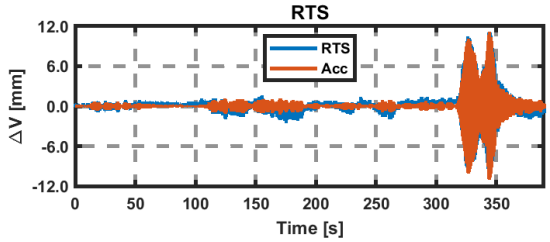

Figure 22. Time Series with event of students jumping (320 s - 360 s).

While the ambient movement of the bridge is very small, a group of people excite the bridge of about 10 mm. Both, ambient and artificial motion can be tracked by the RTS. It has to be said that the accelerometer data is more flattened because it needs to be integrated twice to derive the movement which acts as a low pass filter.

In Figure 23 the FFTs of the time series above are shown. Both, the RTS and accelerometer, are capable of finding the eigenfrequency of the bridge of 1.74 Hz.

As it was shown, it is possible, to derivate the eigenfrequency from big amplitudes. Figure 24 shows the time series of the data, were the bridge was excited by two people, resulting in lower amplitudes.

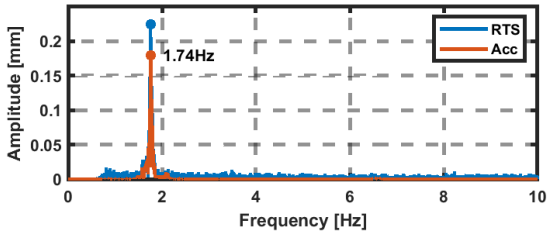

Figure 23. FFT of RTS and Acceleration sensor while 15 students jumping on the bridge.

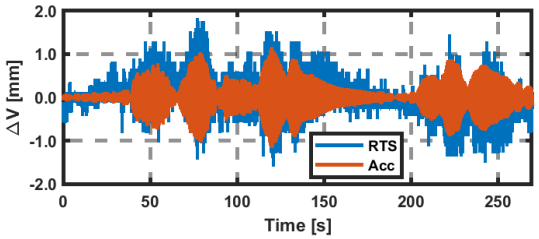

Figure 24. Time series of RTS and acceleration sensor while 2 people jumping on the bridge.

The jumping on the bridge generates amplitudes up to 1 mm. While the filtered acceleration data shows very homogenous movements, the RTS seems to drift a bit over time. This can be bounded to different loadings of the bridge as there were still people crossing the bridge during the experiment. Anyway, it can be seen, that the RTS is capable of following the motion.

In Figure 25 the FFTs of the time series shown above is displayed.

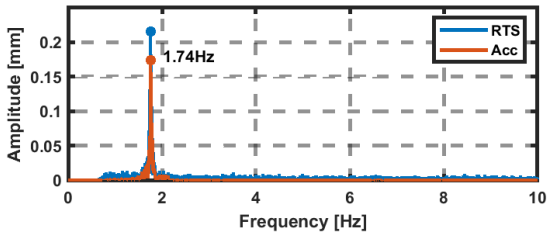

Figure 25. FFT of RTS and Acceleration sensor while two people jumping on the bridge.

Both sensors are capable of finding the eigenfrequency of 1.74 Hz again. Therefore, it can be said that motion significantly higher than the atmospheric disturbances can be detected by the RTS and concluded to the eigenfrequency of an object.

IV. Conclusion

It is shown in this paper, that GNSS and RTS with a sampling rate of 20 Hz is a useful technology for dynamic monitoring of civil structures, where frequencies of less than 10 Hz are expected.

For GNSS a reference station providing 20 Hz is advantageous, especially for low amplitudes. At lower reference station data rate, artefacts in the frequency domain do occur.

If there is no significant oscillation in the data, the GNSS data noise is equally distributed over the frequency domain. If there is a significant oscillation in the data, the frequency determination was very accurate compared to the LTS data. This was shown in the tests at the laboratory with the shaker but also at the footbridge. This frequency determination worked well for high amplitudes (10 mm) but also for low amplitudes (1 mm). It has to be mentioned that the amplitude calculation differed from the LTS data, especially between 2 Hz and 8 Hz in the range of a few millimetres.

For RTS measurements the standard deviation of no movement is depended on various influences like distance to target, surface and surrounding of the signal path and weather.

The frequency determination was very accurate compared to the acceleration sensor data and LTS data. Unfortunately, the RTS cannot hold its sampling rate at high frequencies (~ 9 Hz) and high amplitudes (~ 6 mm), were it dropped to 16 Hz. Having a closer look at amplitudes at certain frequencies, amplitudes derived from RTS data are tendentially too high. It is shown, that the use of RTS in dynamic observation procedure is possible, but there are some inner and outer influences that need to be considered.

V. Outlook

This paper covered the results of accelerations in vertical direction. Further investigations will be carried out in horizontal directions.

References

Górski, P. (2017). Dynamic characteristic of tall industrial chimney estimated from GPS measurement and frequency spe decomposition. *Engineering Structures*, *148*, pp. 277-292.

Im, S. B., Hurlebaus, S., and Kang, Y. J. (2013). Summary review of GPS technology for structural health monitoring. *Journal of Structural Engineering*, *139*(10), pp. 1653-1664.

Le Thi, N., Männel, B., Jarema, M., Seemala, G. K., Heki, K., and Schuh, H. (2021). Selection of an optimal algorithm for outlier detection in GNSS time series. In *EGU General Assembly Conference Abstracts* (pp. EGU21-1598).

Leica (2020). Data Sheet of Leica MS60

Lienhart, W., Ehrhart, M., and Grick, M. (2017). High frequent total station measurements for the monitoring of bridge vibrations. *Journal of applied geodesy*, *11*(1), pp. 1-8.

Moschas, F., and Stiros, S. (2011). Measurement of the dynamic displacements and of the modal frequencies of a short-span pedestrian bridge using GPS and an accelerometer. *Engineering structures*, *33*(1), pp. 10-17.

Nischan, T. (2016): GFZRNX - RINEX GNSS Data Conversion and Manipulation Toolbox. GFZ Data Services. DOI: 10.5880/GFZ.1.1.2016.002

Shannon, C. E. (1949). Communication in the presence of noise. *Proceedings of the IRE*, *37*(1), pp. 10-21.

Shen, N., Chen, L., Liu, J., Wang, L., Tao, T., Wu, D., and Chen, R. (2019). A review of global navigation satellite system (GNSS)-based dynamic monitoring technologies for structural health monitoring. *Remote Sensing*, *11*(9), 1001.

Takasu, T. (2011). RTKLIB: An open source program package for GNSS positioning.

Yi, J., Zhang, J. W., and Li, Q. S. (2013). Dynamic characteristics and wind-induced responses of a super-tall building during typhoons. *Journal of Wind Engineering and Industrial Aerodynamics*, *121*, pp. 116-130.